Current reversal and associated variability within the Corsica Channel: the 2004 case study

Roberta Sciascia[a,*], Marcello G. Magaldi[a,b], Anna Vetrano[a]

[a] *Istituto Scienze Marine (ISMAR), Consiglio Nazionale delle Ricerche (CNR), Sede Secondaria di Lerici, Forte Santa Teresa, Lerici (SP), 19032, Italy*
[b] *Johns Hopkins University, Department of Earth and Planetary Science, Baltimore, MD, USA*

Abstract

Flow reversals within the Corsica Channel, a strait East of Corsica, are investigated with a realistic, high-resolution (~ 1.5 km) numerical setup simulating the year 2004. The simulations compare well with available water mass transport estimates resulting in an annual mean of 0.49 ± 0.49 Sv. Similarly, the model agrees with hydrographic observations in the area, and current velocity measurements showing a flow in the Corsica Channel predominantly directed northward from the Tyrrhenian to the Ligurian Sea. On top of the well-documented Corsica Channel seasonal variability, a higher-frequency variability can be found throughout the year but more frequently during the summer season. This temporal variability, highest close to the western flank of the Channel, is of the order of a few days to a week and associated with reversals of the currents. We find that this variability is ascribed to periodic intrusions of the West Corsica Current on the Eastern side of the Island. Moreover, our findings suggest the importance, of a so-far neglected, across-channel variability of the meridional velocity throughout the

*Corresponding author: R. Sciascia (roberta.sciascia@sp.ismar.cnr.it)

entire 2004. This result potentially questions the single-mooring assumption that has always been at the center of the observational scheme. This assumption holds while looking at low-frequency/seasonal variability but fails when focusing on higher-frequency variability.

Keywords: numerical modeling, high-frequency variability, Corsica Channel, water mass transport

---

1. Introduction

The Corsica Channel is a narrow ($\sim$ 32 km) and relatively shallow (maximum depth $\sim$ 430 m) Mediterranean strait located between the Corsica and Capraia Islands and connecting the Tyrrhenian and Ligurian Seas (Figure 1). The area around the Channel is characterized by a well-known mean cyclonic circulation (Millot, 1999), affecting both the surface layer filled by waters of Atlantic origin, the Modified Atlantic Water (denoted MAW hereinafter) and the layer below of Levantine Intermediate Water (denoted LIW hereinafter).

The cyclonic circulation consists of two currents mainly directed northward on both sides of Corsica, the Western and Eastern Corsica Currents (respectively denoted WCC and ECC hereinafter), which merge north of the Channel forming the so called Ligurian (or Northern) Current (Figure 1a). The two currents are characterized by different water properties (Astraldi et al., 1990). A temperature difference between the two sides of the island is found throughout the year with warmer waters on the eastern side and colder ones on the western side (Astraldi et al. 1990, and references therein). Salinity differences (i.e. saltier ECC compared to the WCC) are visible and more pronounced in winter than in summer (Astraldi et al., 1990).

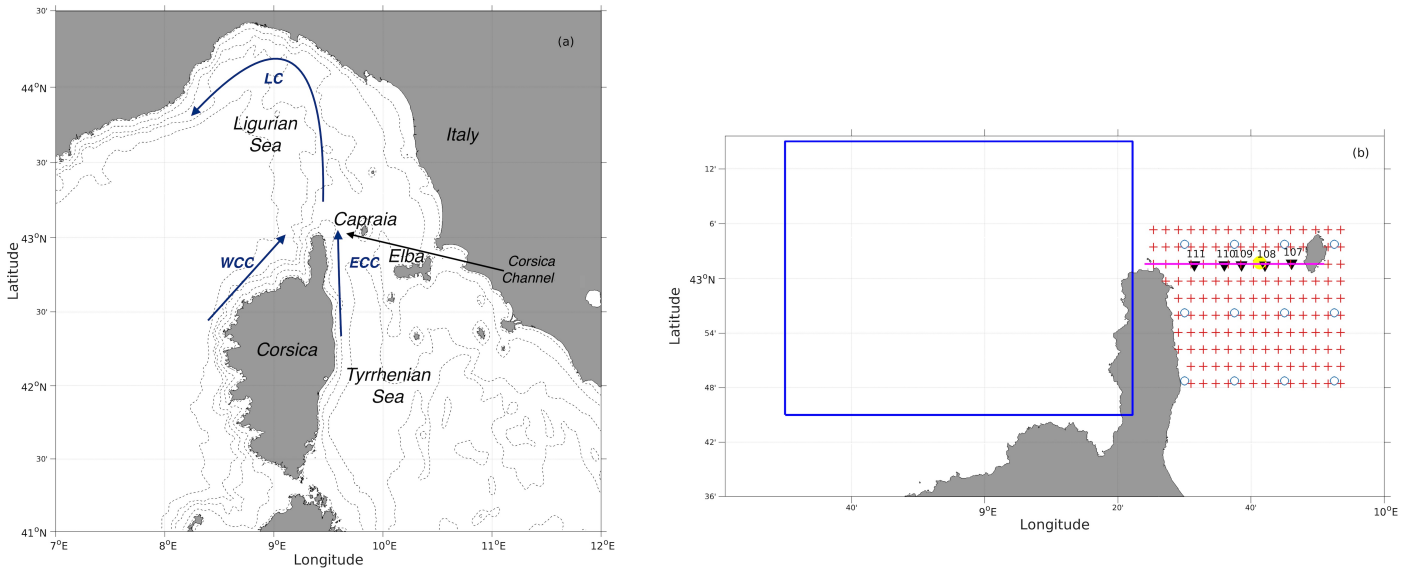

Figure 1: Study area: (a) The Tyrrhenian and Ligurian basins with main circulation branches. Dashed black lines represent bathymetry contours (20, 100, 500, 1000, 2000 and 3000 meters). (b) Zoom on the Corsica Channel region. The blue box indicates the area where wind averages are performed (see Section 4). The horizontal magenta line indicates the LIME-ROMS Corsica Channel transect used throughout the paper (43.0256°N, 9.40 − 9.85°E). The yellow circle denotes the location of the Corsica Channel mooring. Black triangles and relative numbers indicate the CTD casts from the MFSTEP1 cruise. Blue circles and red crosses indicate the numerical grids of MFS and LIME-ROMS, respectively. For visualization purposes both meshes are plotted every second grid point.

The dynamics within the Corsica Channel are important for different reasons. First, they may influence in the Mediterranean Deep Water Formation process as they directly affect the properties of the Ligurian Current, known to modulate the supply of salt by lateral advection in the convection areas (the so-called preconditioning, see Schroeder et al. 2010). Second, they have an impact on biological processes and species distribution in the area: Astraldi et al. (1995) show that the Channel can act as a biological choke point between the Tyrrhenian and Ligurian Seas. Warm-water species of Tyrrhenian origin can be found in the cold Ligurian waters when a northward flow is registered through the Channel. On the contrary, the two basins are biologically separated in presence of a weaker flow in the same Channel (Aliani and Meloni, 1999). Third, they have practical implications on the dispersal of substances and pollutants: different observational and numerical studies (Aliani and Molcard, 2003, Suaria and Aliani, 2014, Suaria et al., 2016, Fossi et al., 2017) show that floating debris tend to accumulate in the area around the Corsica Channel.

The low-frequency variability in the Channel is well established in the literature. It is dominated by a seasonal signal, with stronger northward currents and transports through the Channel during winter. Currents are instead weaker and water mass transports get to near-zero values in summer (Astraldi and Gasparini, 1992). The interannual variability of this signal is related to the state of the North Atlantic Oscillation index as shown by Vignudelli et al. (1999). According to Astraldi and Gasparini (1992) and Vignudelli et al. (2000), seasonal and interannual variabilities are due to a sea surface slope of steric origin associated with the difference in density

between the Ligurian and Tyrrhenian Seas.

Overall, the flow within the Channel is directed northward resulting in positive annual mean transport values oscillating between 0.54 and 0.7 Sv (1 Sv $\equiv 10^6$ m^3/s) in different years (Astraldi and Gasparini, 1990, 2013). These estimates have been observationally determined by a single mooring located in the deepest part of the Channel (Astraldi and Gasparini, 1990, Astraldi et al., 1990). The single mooring configuration is unable to explore the across-channel variability of the horizontal currents but, thanks to the presence of four current meters, it is able to describe their vertical profiles. The underlying assumption in producing these estimates has always been that, compared to the vertical changes, the across-channel variability is small and can be neglected. As a result, the single mooring configuration has been considered adequate enough to estimate the exchanges between the Tyrrhenian and Ligurian basins with enough accuracy (Vignudelli et al., 2005).

Less attention has been historically put in the high-frequency variability (order of a few days to a week) of the same currents. Vignudelli et al. (1999) report several episodes of current reversals across the whole water column in the observations. Manzella (1985) and Pierini and Simioli (1998) suggest that high-frequency oscillations in the order of a few days are wind-driven and, in some cases, comparable to the low-frequency and seasonal signals. Seasonal signatures and evidences of current reversals in the Corsica Channel are also found in satellite observations (Bouffard et al., 2008, Ciuffardi et al., 2016). In particular, Ciuffardi et al. (2016) show that reversals occur in the Channel mostly in summer and early fall and may be associated with the

location of the so-called Ligurian anticyclone.

Little work has been done in modeling the Corsica Channel at high-resolution: many Northwestern Mediterranean models have either coarse resolution (Herbaut et al., 1997, Myers and Haines, 2000, Fernández et al., 2005) or focus on other areas such as the Gulf of Lion (Echevin et al., 2003, Mounier et al., 2005, Damien et al., 2017), the Ligurian (Casella et al., 2011) or Tyrrhenian (Vetrano et al., 2010) Seas.

Due to the low resolution of most of the observations and models so far considered in the area, the kinematic description of the flow reversals in the Corsica Channel is largely unknown and is the ultimate focus of this study. We use a comprehensive joint observational–modeling approach. On one hand, we use mooring and hydrological data in the Channel. On the other hand, we compare model outputs from two different modeling systems, at different resolutions. The first is the widespread Mediterranean Forecasting System (MFS) with a relatively coarse resolution of $1/16^\circ \times 1/16^\circ$. We then set up and run a four-time, $1/64^\circ \times 1/64^\circ$, higher-resolution configuration of the Northwestern Mediterranean Sea (LIME-ROMS). We decide to focus on the year 2004 for three different practical and scientific reasons. First, more observations are available in 2004 with respect to other years, allowing for better comparisons with models. Second, 2004 is the first year when coarser MFS model outputs are available. Third, 2004 is dynamically important as it is the last year before the abrupt shift registered in the intermediate and deep layers of the Western basin (Schroeder et al., 2016).

The aim of this study is twofold: a) to check the reliability and realism of the new high-resolution numerical model in the Corsica Channel, where

ground-truth observations are available, and b) to extend the analysis and the understanding of the observed flow reversals within the Channel with the help of the LIME-ROMS simulations. Specifically, the questions addressed in this work are the following: 1) How realistic are the simulated fields near the Channel using a state-of-the-art high-resolution model? 2) Can the model reproduce the observed seasonal variability in the water mass transport through the Channel? 3) Are Corsica Channel reversals present and important in the model solutions? 4) What is their spatial location? 5) Is a single mooring adequate enough to capture their variability?

The rest of the paper is organized as follows. The principal characteristics of the LIME-ROMS model and the details of the configurations used in this study along with the observational and numerical data used for comparison are presented in Section 2. Results and model validation are reported in Section 3, followed by a discussion in Section 4. Conclusions are drawn in Section 5.

2. Methods

2.1. Observations within the Corsica Channel

2.1.1. Hydrographic transects

In 2004 two oceanographic cruises sampled the area around the Corsica Channel providing temperature and salinity data. The first one (MEDGOOS08, May 8-21) mostly surveyed the Tyrrhenian Sea, while the second (MFSTEP1, September 18-30) surveyed the Ligurian Sea from the coasts of Italy to those of France.

In both campaigns the continuous vertical profiles of conductivity, temperature and pressure were acquired from surface to bottom with a CTD-rosette (Conductivity-Temperature-Depth-rosette) system consisting of a CTD SBE 911 plus, and a General Oceanics rosette with 24 Niskin bottles for water samples. Accuracies for temperature and conductivity measurements are 0.001°C and 0.0003 S m^{-1}, respectively. Instruments were calibrated before and after each cruise at the Centre for Maritime Research and Experimentation (CMRE, former NURC-NATO) in La Spezia, Italy.

The area around the Corsica Channel transect was sampled with 10 and 5 CTD casts for the MEDGOOS08 and MFSTEP1 cruises, respectively. However, all 5 CTD casts of the MFSTEP1 cruise are in the deepest part of the Channel where the mooring is located (Figure 1b), while only 2 CTD casts of the MEDGOOS08 cruise are available for the same region. The remaining 8 CTD casts of the MEDGOOS08 cruise extend northeastward from the Capraia Island to the coasts of Italy. As the focus is on the Corsica Channel and the MEDGOOS08 overall picture in the Channel is consistent with that provided by the MFSTEP1 survey, in the following we will only show data from the MFSTEP1 cruise.

Potential density (σ_θ) and potential temperature (θ) fields, referenced to the sea surface, were calculated from the acquired vertical profiles. Vertical property sections were then constructed by interpolating the data onto regular grids, with a resolution of 1/64° (1.5 km, approximately) in the horizontal and 5 m in the vertical and using a Laplacian-spline interpolation scheme. The bottom topography for the sections is interpolated from the 1 arc-minute ETOPO1 product (Amante and Eakins, 2009).

2.1.2. *Velocity measurements and water mass transport estimates*

Currents within the Channel have been observed for quite a long time from a long-term mooring maintained by CNR-ISMAR since 1985 (Astraldi and Gasparini, 1990, Astraldi et al., 1990). To date, these observations are the longest record of continuous velocity measurements in the Mediterranean Sea. The mooring is located west of Capraia, at 43.029N - 9.688E (Figure 1b, yellow circle) where bathymetry steepens deeply up to 430 m. It has been historically equipped with Aanderaa RCM current meters, routinely calibrated by the manufacturer before and after deployment, i.e. about twice per year. After March 2010, the mooring has been substantially rearranged with the introduction of Teledyne RDI Acoustic Current Doppler Profilers.

During 2004, four RCM-9 Aanderaa current meters were centered at the approximate depths of 50, 100, 300 and 380 m and currents have been sampled every hour to produce daily averages. Current meters absolute accuracy is 0.0015 m s^{-1} and 5° for speed and direction, respectively. System failures resulted in data gaps at the depths of 100 and 300 m (see Section 3.3). Temperature sensors are present on all four current meters, while only the deepest one is equipped with a salinity sensor. However, the salinity sensor had some calibration issue for part of 2004 resulting in inaccurate readings.

2.1.3. *Water mass transport through the Corsica Channel*

To calculate the evolution of the total water mass transport trough the Corsica Channel from the current meter data we consider only the meridional component of the velocity field. Data gaps at 100 m, v_{100}, have been reduced by the following linear combination of nearby velocities v_{50} and v_{300}, i.e. the

meridional velocities at 50 and 300 m when both available:

$$v_{100} = \alpha_0 + \alpha_1 v_{50} + \alpha_2 v_{300} \quad (1)$$

where $\alpha_0 = 0.5129$, $\alpha_1 = 0.5341$ and $\alpha_2 = 0.3061$ are coefficients determined by a multivariate regression analysis of the meridional daily velocity time series spanning from November 1, 1985 to December 31, 2007. Nevertheless, in 2004 water mass transport estimates during the period from August 7 to September 23 cannot be provided as both v_{100} and v_{300} data are missing.

The Channel cross-sectional area is regularly shaped in the horizontal and very narrow below 100 m depth. Due to this simplified geometry, current measurements at each depth have always been assumed to be representative of a specific portion of the cross-sectional area, ignoring their horizontal variability. The associated cross-sectional areas are 1.875 km^2 for the current meter located at 50 m and 1.743, 1.211, 0.380 km^2 for the current meters at $100, 300, 380$ m respectively. The single mooring solution of the Corsica Channel has always been considered adequate enough to estimate the exchange of water masses between the Tyrrhenian and Ligurian basins with enough accuracy (Vignudelli et al., 2005).

2.2. Coarse resolution numerical outputs

Model daily outputs at relatively coarse resolution come from the Mediterranean Forecasting System (MFS, SYS4a3 version) downloaded in the past from the myOcean EU-project web portal and currently substituted by the Copernicus Marine Environment Monitoring Service (CMEMS, `http://marine.`

copernicus.eu). The model horizontal grid resolution (Figure 1b, blue circles) is $1/16° \times 1/16°$ ($6-7$ km, approximately) while the vertical dimension is resolved with 72 unevenly spaced z-levels. The hydrodynamical model is based on the Nucleus for European Modelling of the Ocean - Océan PArallélisé (NEMO-OPA, http://www.nemo-ocean.eu, 3.2 version, Madec et al. 1998) and uses its data assimilation capability via the OCEANVAR scheme developed by Dobricic and Pinardi (2008). The assimilated ocean measurements include satellite (sea level anomalies, sea surface temperature) and in situ data (Argo floats, CTDs and XBTs). Satellite OA-SST (Objective Analyses - Sea Surface Temperature) data are used to correct surface heat fluxes, previously computed by bulk formulae, with a relaxation constant of 40 W m^{-2} K^{-1}.

The reader is referred to Delrosso et al. (2016) for a description of the numerical MFS-SYS4a3 setup and its validation.

MFS estimates of the water mass transport between the Tyrrhenian and Ligurian basins are calculated using data from all grid points of the cross-sectional area closest to the Corsica Channel mooring location and the MF-STEP1 transect (Figure 1b). The same grid points are used for comparison with the hydrodynamical observations.

2.3. High-resolution simulations

The dynamics within the Ligurian and Tyrrhenian Seas are simulated using the Regional Ocean Modelling System (ROMS) (Shchepetkin and McWilliams, 2005) specifically the Rutgers University kernel which was first introduced by Haidvogel et al. (2000). ROMS is chosen for different reasons: first for the terrain-following *"sigma"*-coordinate vertical grid that allows a good vertical

resolution in both shallow and deep areas, e.g. the Tuscanian shelf and the Tyrrhenian Sea, respectively (Figure 1a). Second for its ability to run with zero explicit numerical viscosity: ROMS advection operator can rely on a third-order, upstream-biased scheme (Shchepetkin and McWilliams, 1998) and uses the smallest possible numerical dissipation to allow the growth of realistic instabilities (Ilıcak et al., 2012). This feature is crucial for high-resolution simulations where small-scale processes need to be retained and not numerically dissipated. Third, ROMS has useful features that will be exploited in future works, namely sediment and biological modules and the two-way coupling to atmospheric models (Warner et al., 2005). Finally, previous realistic and successful ROMS configurations have been set up in different areas of the Mediterranean (Chiggiato and Oddo, 2008, Carniel et al., 2009, Magaldi et al., 2010, Casella et al., 2011, Iermano et al., 2016).

ROMS is setup under the framework of the Ligurian Integrated Modelling Effort (LIME-ROMS, hereinafter) put forth at CNR-ISMAR. LIME-ROMS numerical domain is discretized with an horizontal grid of 590×314 points. The mesh is unevenly spaced and the most resolved area, which includes the Corsica Channel, has a horizontal resolution of $1/64° \times 1/64°$, for a nominal horizontal resolution of about 1.5 km (Figure 1b, red crosses). The vertical dimension is discretized by 50 *sigma* layers for a total of more than 9 million grid-points. Increased near-surface resolution is achieved using stretching factors $\theta_s = 6.5$ and $\theta_b = 2.5$ for the surface and the bottom respectively. The ROMS generic length scale algorithm (Umlauf and Burchard, 2003) is used to define a $\kappa - \epsilon$ turbulence closure in the vertical with Canuto-A stability functions (Canuto et al., 2001). Ilıcak et al. (2008) showed that

$\kappa - \epsilon$ turbulence closure is well suited to represent exchange channel flow. Zero-explicit numerical viscosity and diffusivity are used in the horizontal. Third-order upstream-biased and MPDATA schemes are used for momentum and tracer advection, respectively. Raw bathymetry data are taken from the 1 arc-minute ETOPO1 product (Amante and Eakins, 2009) and interpolated on the numerical grid. The bathymetry field $h(x, y)$ then undergoes several passes of a smoothing filter to reduce the $r-$factor (Haidvogel and Beckmann, 1999), defined as $r = \Delta h/2h$. A maximum value of $r = 0.35$ is chosen to reduce pressure gradient errors while retaining important topographic features characterizing both Ligurian and Tyrrhenian Seas, namely canyons and seamounts. Minimum model depth is set to 10 m. Bottom stresses are calculated using a quadratic bottom drag coefficient of $C_d = 3 \times 10^{-3}$. Open boundaries are located at southern and eastern side of the domain while no-slip conditions are applied to the closed boundaries.

The LIME-ROMS high-resolution simulation starts from a 2-year climatological spinup and covers the whole 2004. The 2-year spinup starts from the MFS monthly average of January 2004 and is forced at the surface by the monthly climatological wind stresses, net heat and freshwater fluxes obtained from the $1^\circ \times 1^\circ$ Comprehensive Ocean-Atmosphere Data Set climatology (COADS, Worley et al., 2005). The spinup open boundary conditions use the 2004 monthly values obtained averaging the MFS outputs. After the 2-year spinup, realistic surface forcing for 2004 comes from the 3-hourly, 0.25° horizontal resolution ERA-Interim reanalysis fields (Dee et al., 2011) available at the `http://apps.ecmwf.int/datasets/data/interim-full-daily` link. Atmospheric data include wind velocity at 10 m, surface pressure, sur-

face air temperature and relative humidity both at 2 m, solar shortwave and downwelling longwave radiation, and rain fall rate. Momentum, freshwater and heat fluxes are all calculated by the model using the atmospheric data and the surface model state via bulk formulae (Fairall et al., 1996a,b).

Daily open boundary values are derived from the coarser MFS SYS4a3 product and used to specify the incoming characteristics via Flather conditions (Blayo and Debreu, 2005) while an implicit Chapman radiation condition (Chapman, 1985) is used for the sea surface elevation. Normal barotropic velocities are imposed in order to ensure no net inflow, while radiation conditions are applied at the two open boundaries for baroclinic velocities and tracers.

MFS monthly averages for the 2004 year are also used for baroclinic velocities and tracers (Blayo and Debreu, 2005) and nudged with a time scale of 6 h at the boundary. The nudging is milder and the time scale increases toward the interior of the domain to reach the maximum value of 10 days. The use of milder time scales and of monthly averages limits the impact of the MFS solutions and better allows LIME-ROMS to develop its own dynamics even in the nudging portion of the domain. No nudging is performed over the most resolved interior region and over the area of interest. Model solutions are stored every six hours.

As for the coarser MFS model, LIME-ROMS grid points closest to Corsica Channel mooring and MFSTEP1 transect are used for comparison with the hydrodynamical observations and to provide estimates of the water mass transport through the Channel.

3. Results

In this section, both coarse and high-resolution models are compared to the observations. We begin with the 2004 hydrographic data taken within the Corsica Channel and the general known circulation. A direct comparison between the measured and modeled velocities at the Corsica mooring is then provided together with a comparison of the water mass transport through the Channel. The observations are eventually put into temporal context with the help of the high-resolution LIME-ROMS model.

3.1. Hydrographic sections

The upper panels of Figure 2 show the hydrographic data from the MF-STEP1 cruise taken on September 24, 2004. Observed values are typical of the Corsica Channel, as reported for the 2004 year by Vetrano et al. (2010, cf. their Figure 2): MAW waters occupy the entire surface layer of the section, centered around the salinity minimum of 38 at about 75 meters of depth. LIW waters are directly below the MAW layer, characterized by potential densities and salinities larger than 28.9 and 38.5, respectively. It should be noted that the vertical distribution of the current meters is similar to that used in the past, to capture the MAW (LIW) layer with the top (bottom) two instruments (Vignudelli et al., 2000).

The observations show a warm and salty well-mixed layer which extends down to a depth of 50 meters followed by a sharp thermocline. Below the thermocline, waters in the Channel are colder with potential temperatures of about 14 °C.

The general hydrographic structure is maintained in both MFS (Figure

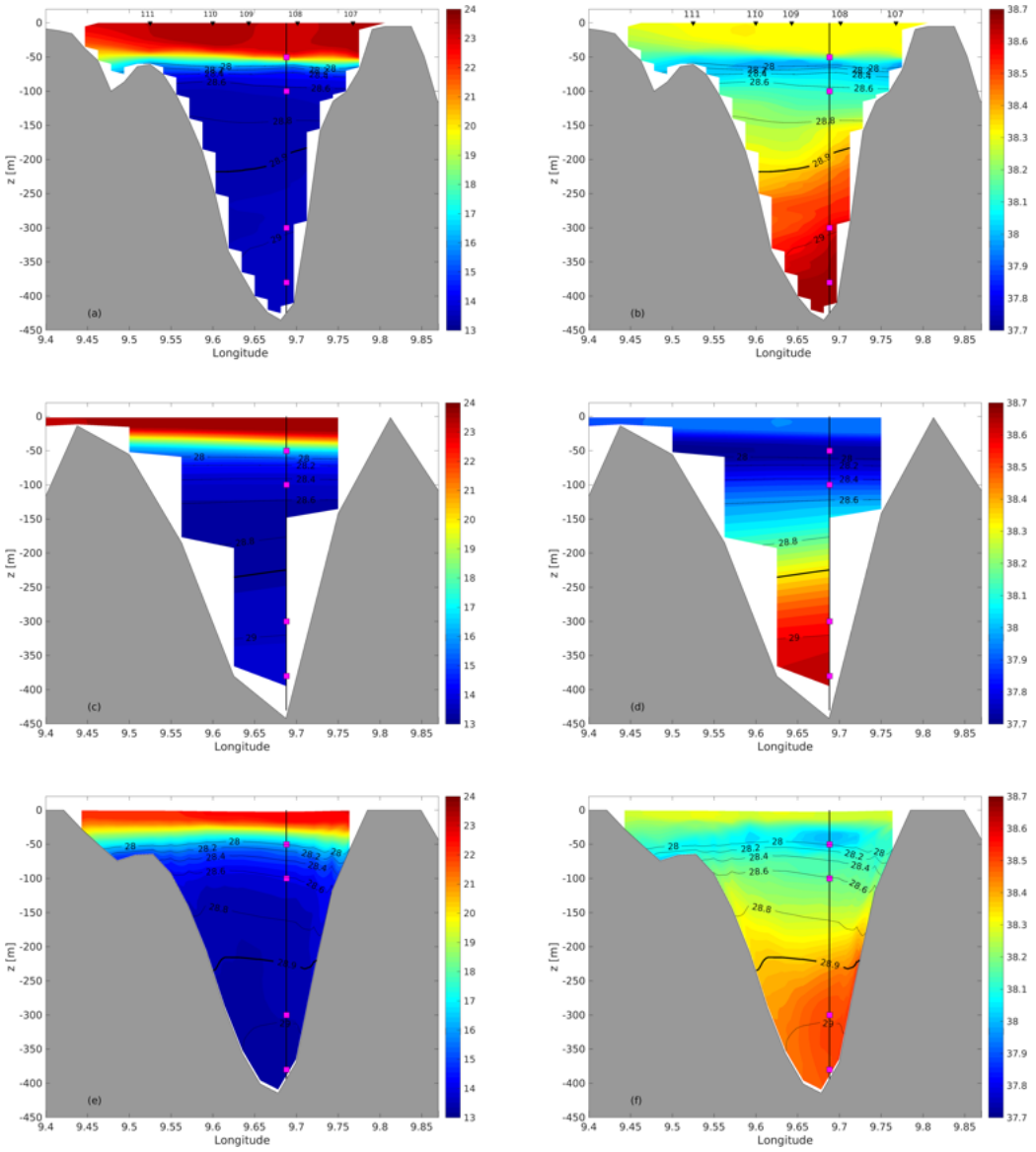

Figure 2: Hydrography on September 24, 2004 within the Corsica Channel. Potential temperature θ (°C) and salinity S for: (a-b) the observations during the MFSTEP1 cruise; (c-d) MFS and (e-f) LIME-ROMS simulations. Vertical lines and magenta squares indicate the position of the Corsica Channel mooring and the locations of the four current meters. Black lines indicate potential density contours (kg/m^3).

2, central panels) and LIME-ROMS (Figure 2, lower panels) sections, with the interface between MAW and LIW layers located in the same position of the observations, i.e. at about 200 meters of depth. Some differences may be noted, however. Both models show a shallower well-mixed layer and a gentler thermocline. This is consistent with what has been also recently found in the literature: in the same area, Onken (2017) reports that modeled mixed-layer depths are shallower than in the observations and sensitive to vertical mixing parameterizations, initial and boundary conditions. As a result, contrarily to both models, the top current meter still lies at the lower edge of the warm and salty mixed-layer (Figure 2, upper panels) and is more likely to be affected by the atmospheric forcings than in the simulations. With respect to salinity, LIME-ROMS agrees better with the observations compared to MFS at the surface. Isohalines, and in general isopycnals, are distorted at the boundaries of the Channel. We speculate that this may be due to arrested Ekman layers, described for the first time in (Garrett et al., 1993). Higher resolutions in the Channel, both in the horizontal and vertical dimensions, are needed to check this hypothesis. The coarse-resolution simulation is instead more in line with the observations at the bottom with LIW waters saltier than 38.6. We will assess this apparent inconsistency of the high-resolution LIME-ROMS setup later in the paper.

3.2. General circulation

Figure 3 shows the LIME-ROMS monthly mean of the surface horizontal velocity, vertically-averaged in the first 20 meters of depth, for the months of February (Figure 3a) and August (Figure 3b). The model reproduces the general circulation of the area with the WCC flowing West of the Corsica

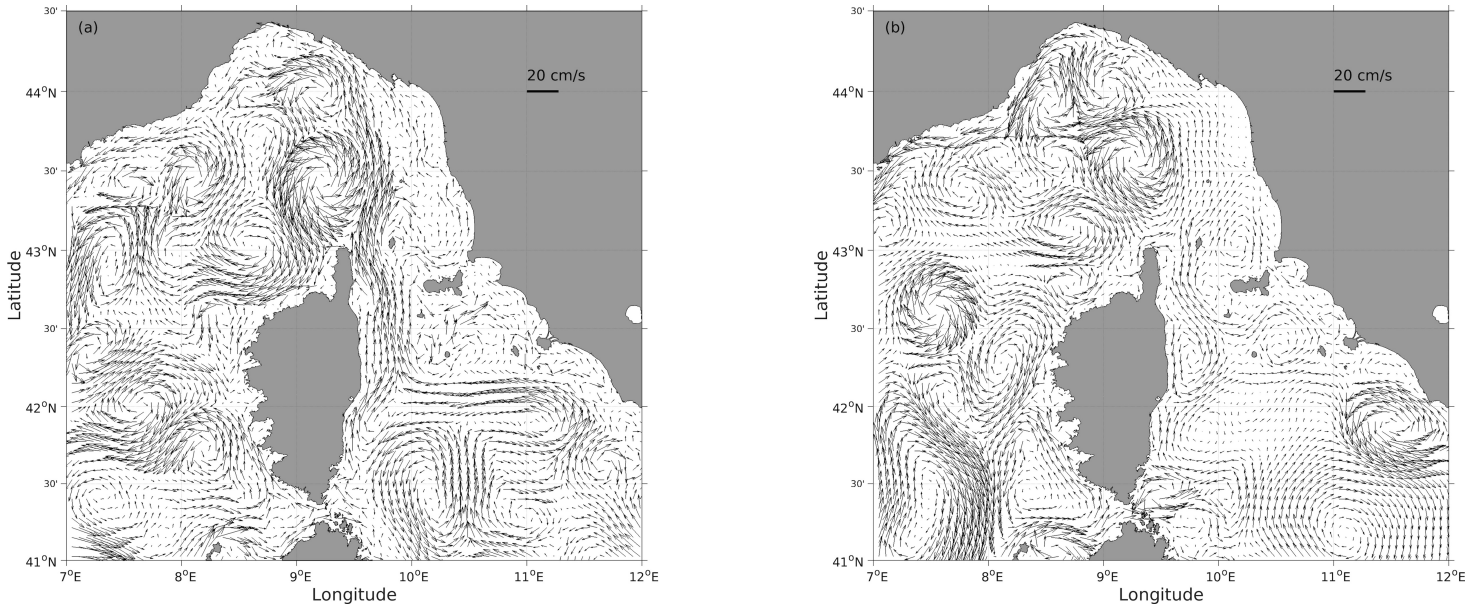

Figure 3: LIME-ROMS monthly mean of the depth averaged (0-20 meters) horizontal velocity for (a) February and (b) August 2004

Island and the ECC on the Eastern side. The two currents merge north of the Island forming the LC that flows along the coasts of Italy and France. Large eddies moving with the large-scale cyclonic circulation of the basin are evident north and west of Corsica, with diameters in the range of 40-60 km. Their dimensions are realistic, being consistent with both the wavelength of the meanders observed from satellite in the same area (Crépon et al., 1982) and the estimate of the deformation radius of the first mode provided by Gasparini and Manzella (1983).

The circulation on the Eastern side is characterized by the known seasonal variability, with a strong northward ECC that occupies the whole width of the Corsica Channel in winter (Figure 3a). Moving southward, other recurrent features, like the Bonifacio cyclone (Artale et al., 1994, Astraldi and Gasparini, 2013) can be found. During February, due to the presence of smaller-scale eddies, the Bonifacio cyclonic structure is not well organized, but rather fragmented in a first zonally-stretched cyclone centered at about 42°N and in a second one with its center at about 10.1°E and 41.3°N. A similar stretching, in both zonal and meridional directions, is reported elsewhere (Astraldi and Gasparini, 2013, Marullo et al., 2013, Rinaldi et al., 2010).

In summer, the ECC flow is weaker and mainly limited to the eastern side of the Channel, veering right north of it, and forming an anticyclonic structure centered around the Capraia Island (Figure 3b). This feature has been named as Ligurian anticyclone (Ciuffardi et al., 2016). It is sampled by satellite-tracked drifters (Poulain et al., 2012) and has a summer and early fall signature (Ciuffardi et al., 2016). In summer the Bonifacio cyclone is paired south with the North Tyrrhenian or Bonifacio anticyclone (Moen,

1984, Rinaldi et al., 2010) but its position and size are not reproduced properly in the LIME-ROMS setup as LIME-ROMS is a free run and does not assimilate sea level anomalies unlike MFS.

3.3. Velocity stick plots

The seasonal and interannual variability within the Corsica Channel has been already assessed thanks to the presence of the long term mooring (Astraldi and Gasparini, 1992, Vignudelli et al., 2000). The currents measurements taken in 2004 confirm the well-known seasonality and are characterized, at all depths, by a stronger flow in winter and spring, and a weaker flow in summer and early fall (Figure 4). The mooring measurements show that in addition to the low-frequency (seasonal) variability of the velocity field, a higher-frequency (period from a few days to a week) signal can be found throughout the year and especially in summer.

The velocities are mainly directed northward and toward the Ligurian Sea with occasional reverse flows (red sticks in Figure 4). In 2004, current reversals become persistent in summer and early fall (i.e. in the period from June 1 to September 30) at the depths of 50 meters. Interestingly enough, both strongest northward (54 cm/s) and southward (27 cm/s) velocities are registered not at the surface but at 300 meters, on May 15 and June 21, respectively. Currents reverse, i.e. moving toward the Tyrrhenian Sea, in 24% of the 2004 days at the depth of 50 meters, where no data are missing. Flow reversals are present at all depths and their occurrence is mostly constant with depth with a slight increase near the bottom.

To compare the real mooring with both pointwise model synthetic current meters, model velocity fields are subsampled at the closest gridpoints

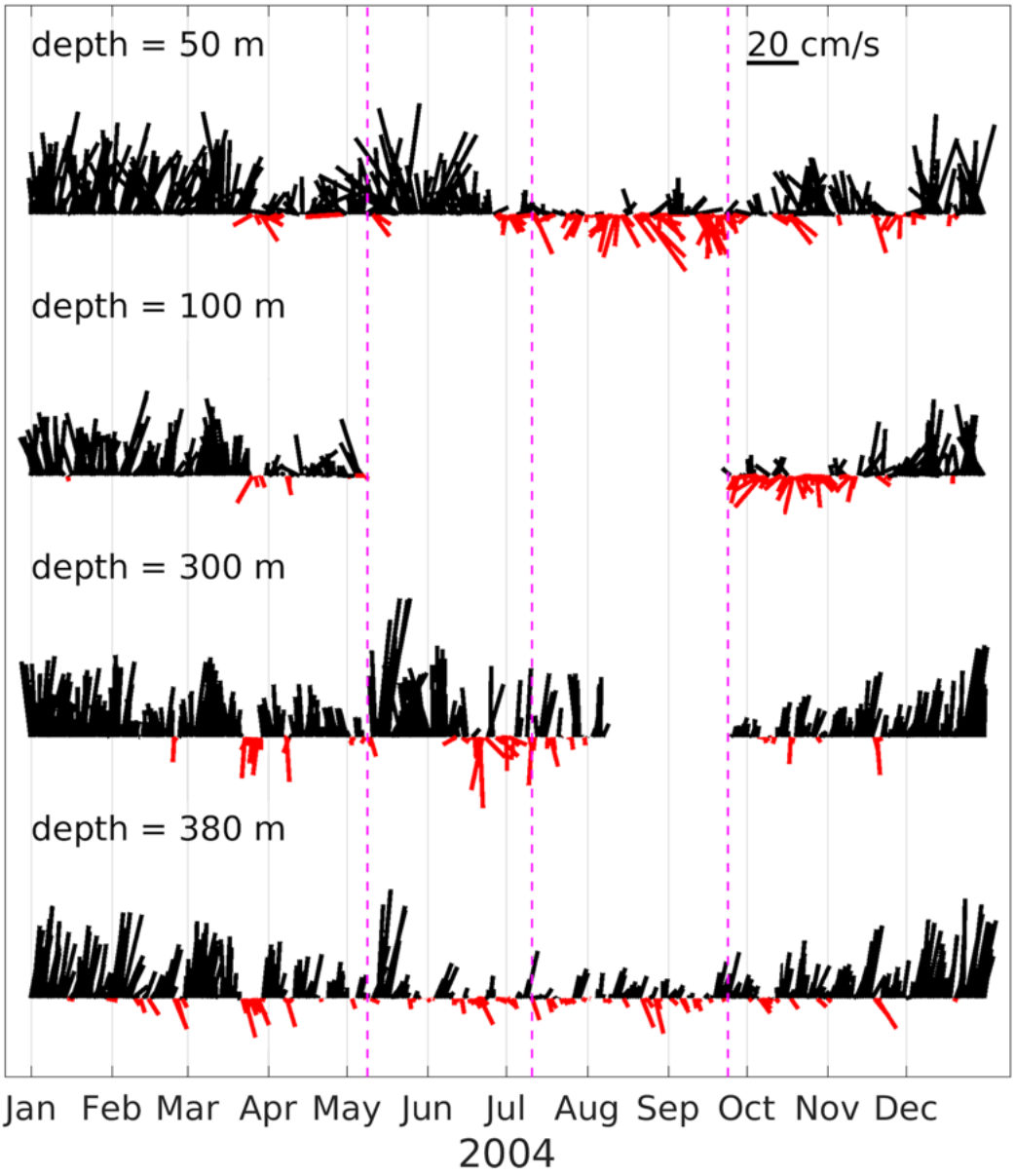

Figure 4: Stick plot of the velocity field from the Corsica Channel mooring at different depths (50, 100, 300 and 380 meters). Magenta vertical lines are relevant to the analysis in Sections 3 and 4 and indicate May 9, July 11 and September 24, 2004.

to the four current meter positions. The seasonal variability found in the observations can be noted also in the MFS simulations (Figure 5). MFS flows are mainly directed northward and characterized by a surface intensification as MFS deep currents are weaker than in the observations. These unrealistic weak deep currents are likely due to the coarse resolution of the model and the poor representation of the Channel bathymetry. In the MFS simulations the flow reverses its northward direction more frequently than the observations. On average, the currents are directed southward in 30% of the 2004 days and, similarly to the observations, the vertical distribution is characterized by more episodes at depth than at the surface (Figure 5).

The high-resolution LIME-ROMS simulations capture the well-known seasonal variability in Channel as well (Figure 6). LIME-ROMS currents are also in better agreement with the observations in terms of magnitude over the whole vertical profile. As in the MFS runs, LIME-ROMS simulations have more reversal episodes than the observations, on average 30% of the 2004 days. LIME-ROMS reversal episodes are reduced at the surface and more frequent at depth (Figure 6).

It is worthy to point out that, looking at all three stick plots, in some occasions and at the mooring location, the flow reverses its direction only at depth like on the first days of June for MFS runs or on May 9 for both observations and LIME-ROMS simulations (first magenta vertical line in Figures 4 and 6). In other cases, the whole water column reverses its direction, like on July 11 for the observations and both numerical models (second magenta vertical line in Figures 4, 5 and 6). We address this important variability in the following.

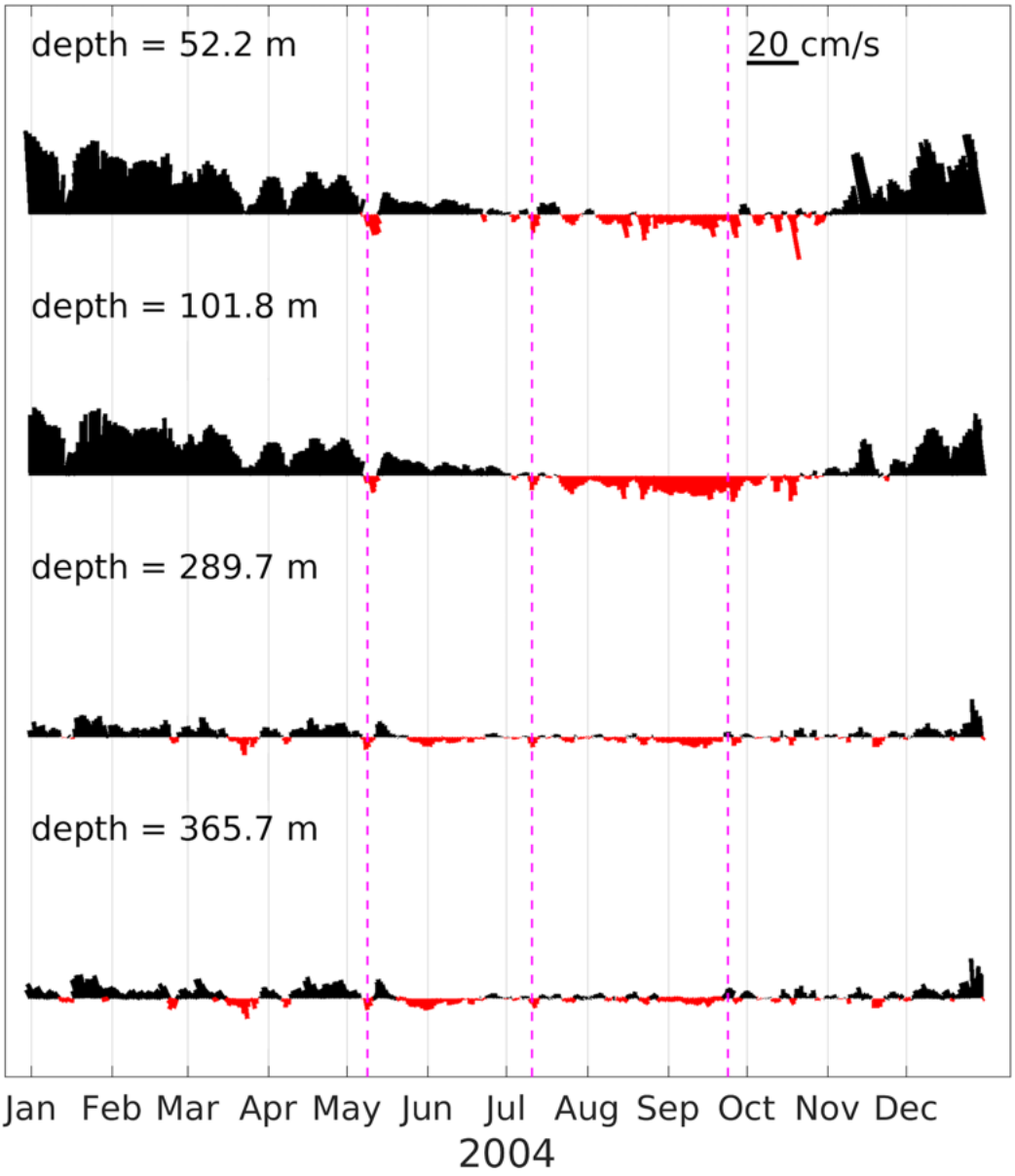

Figure 5: Same as Figure 4 but for the MFS simulations. Note that the data relative to the simulations are obtained from the closest grid points to the mooring longitude and depths.

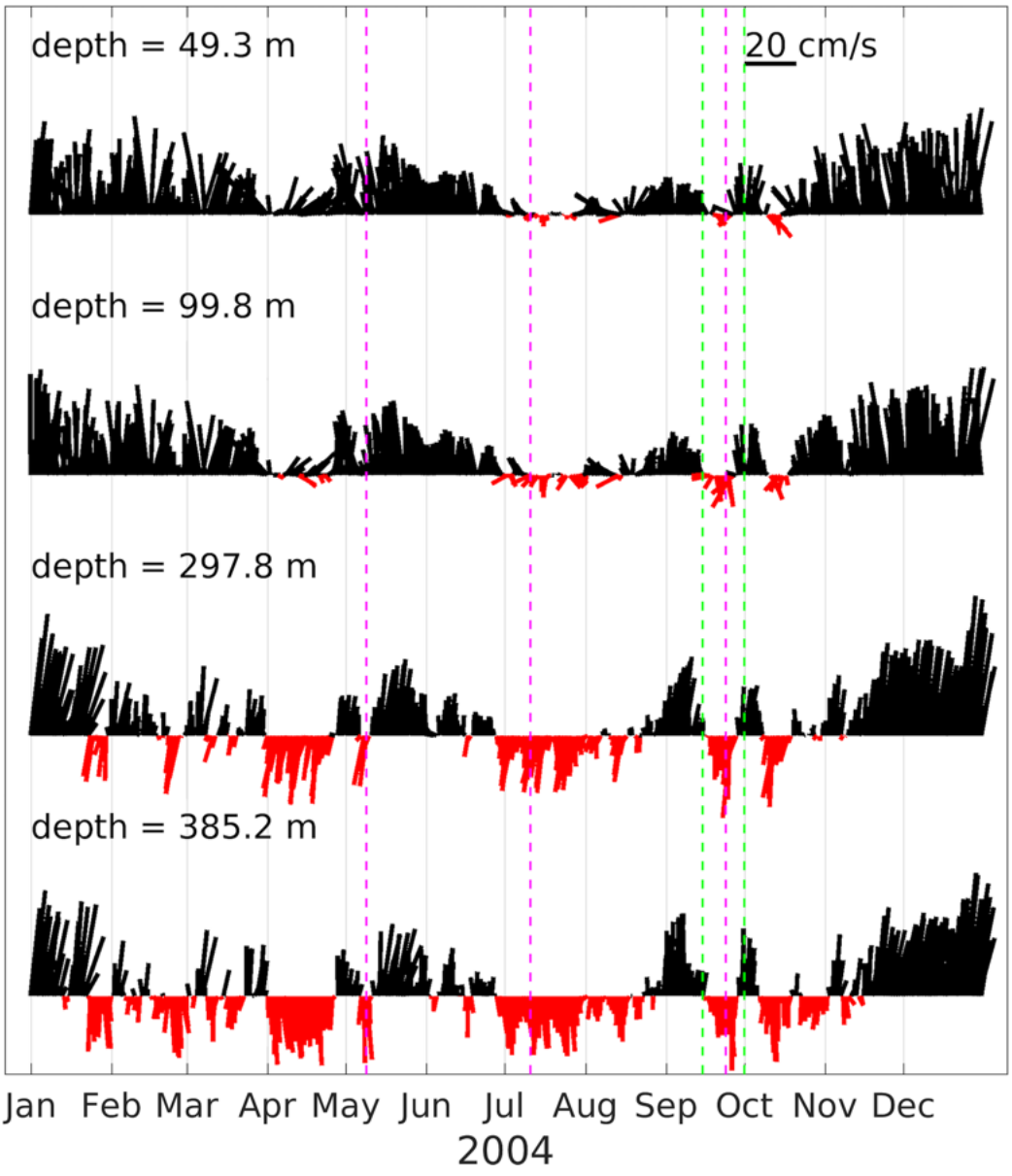

Figure 6: Same as Figure 5 but for the LIME-ROMS simulations. Similarly to the MFS simulations the data relative to the simulations are obtained from the closest grid points to the mooring longitude and depths. Green vertical lines are relevant to the discussion in Section 4 and indicate September 15 and October 1, 2004.

Time series	2004 Water Mass Transport (Sv)	Excluding Aug 9 - Sep 23
OBS	0.54 ± 0.50	0.54 ± 0.50
MFS	0.19 ± 0.30	0.25 ± 0.28
LIME-ROMS	0.49 ± 0.49	0.53 ± 0.49

Table 1: Statistics of the water mass transport through the Corsica Channel from mooring observations (OBS), high- (LIME-ROMS) and coarse- resolution simulations (MFS). The second column reports the transport annual means and standard deviations over the whole 2004. The third column the annual mean excluding from the numerical results (LIME-ROMS, MFS), the data in the period when observations are missing (August 7 - September 23, 2004, see Section 2.1.3).

3.4. Corsica Channel water mass transport

Current meter data from the real mooring are used to calculate the water mass transport through the Channel for the 2004 year as detailed in Section 2.1.3. It is again important to note that, in doing so, the potential across-channel variability of the meridional velocity is neglected. The 2004 observed transport (Figure 7, green line) has a clear seasonal signal with larger values in winter and lower in summer.

Maximum values of about 2 Sv are registered in May, when the current data at 100 m are missing and reconstructed from the two closest current meters, possibly giving rise to anomalously high mass transport values. Minimum values close to -0.5 Sv are instead observed in July. The predominant northward flow at all depths (Figure 4) results in a positive annual mean for the water mass transport through the channel of 0.54 Sv (cf. Table 1), in agreement with the literature annual values of 0.71, 0.65 and 0.54 Sv recorded during three consecutive years (Astraldi and Gasparini, 2013). The observed

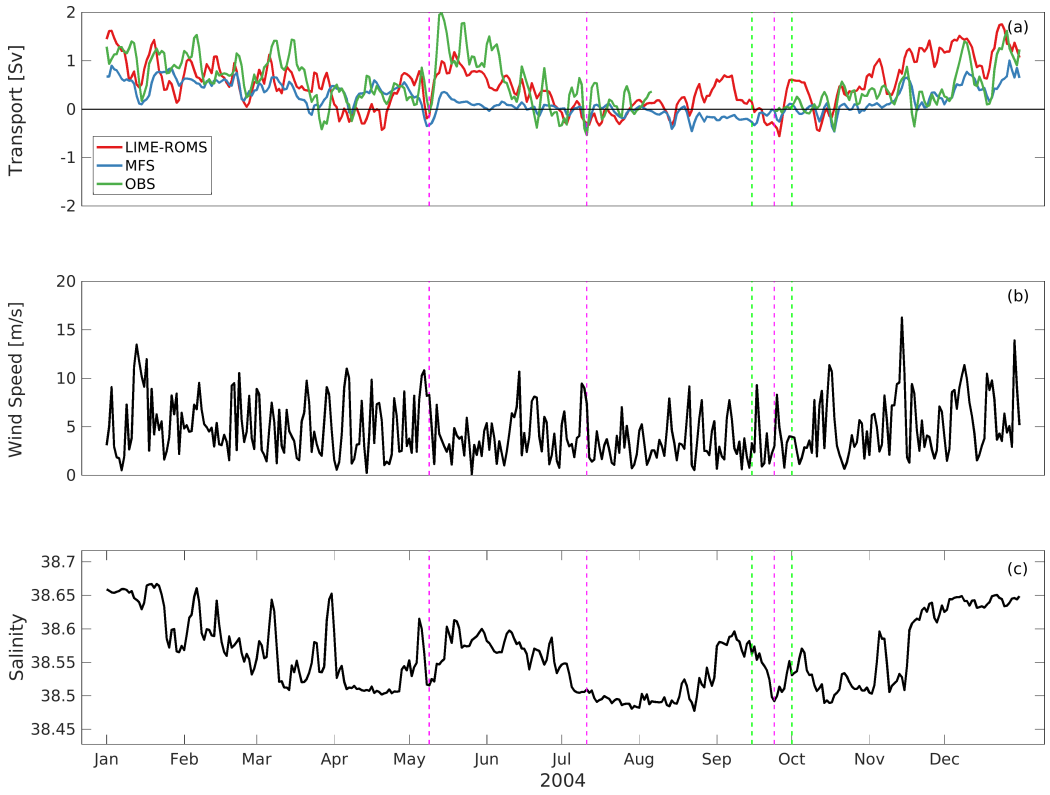

Figure 7: Time evolution for: (a) the water mass transport through the Corsica Channel for LIME-ROMS simulation (red line), observations (green line) and MFS simulations (blue line); (b) ERA-Interim 10 meters zonal wind speed averaged over the blue box indicated in Figure 1b; (c) LIME-ROMS salinity at the location of the deepest synthetic current meter (385.2 meters, see Section 3.3). Magenta and green vertical lines are as in Figures 4, 5 and 6.

variability is significant and the standard deviation of the annual transport is almost equal to the mean value (Table 1).

The modeled water mass transports show similar trends to those computed from the Corsica Channel mooring (Figure 7a). The weak MFS velocities result in lower values for the mean and standard deviation (0.19 ± 0.30 Sv, Table 1). Nonetheless, during some periods, the coarse resolution model shows a better agreement with the observations, for example in spring. On the other hand, the high-resolution LIME-ROMS simulations are able to better capture the high-frequency variability (Figure 7a, red line). In LIME-ROMS, the water mass transport increases in winter reaching peaks of ~ 1.5 Sv, decreases in spring, has its minimum in summer ~ -0.5 Sv and starts increasing again in fall (Figure 7a, red line). As a result, the LIME-ROMS annual transport mean and standard deviation values are 0.49 ± 0.49 Sv, in line with the observations. If the period of the missing observations (August 7-September 23, see Section 2.1.3) is excluded from the the modeled transports, both LIME-ROMS (0.53 ± 0.49 Sv) and MFS (0.25 ± 0.28 Sv) annual transport values are in closer agreement with the observations (Table 1).

Despite the net and mean positive annual values, the 2004 transport curves are characterized by frequent decreases, as well as episodes of negative values through the Channel (Figure 7a) associated with current reversals. In this and the following sections we will focus our analysis on three specific days (vertical magenta lines in Figures 4, 5, 6 and 7), namely on:

- May 9: when observations and both models register at the same time a negative peak in the water mass transport through the Channel;
- July 11: when another negative peak is registered in all three transport

curves together with the minimum value for the observations;

- September 24: when the MFSTEP1 hydrographic data was taken (see Section 3.1) and reversals are registered at all depths in LIME-ROMS.

3.5. Meridional velocity section in the Corsica Channel

To fully take advantage of running the high-resolution LIME-ROMS setup, we compare sections of the dominant component of the velocity field, i.e. meridional velocity, for this configuration (Figure 8). The annual velocity averages are northward/positive, almost uniform over the section (Figure 8a). Weakly positive (0-2 cm/s) averaged meridional velocities are found in some areas, namely the coasts close to Corsica, both at the surface and near the bottom. If the average is performed over the period when the current reversals are more frequent (June 1 - September 30) a southward/negative flow dominates the subsurface area near Corsica and almost the entire section below the depth of 150 meters (Figure 8b). Negative areas are more evident if we look at some of the above mentioned single episodes, like on May 9 and July 11 (Figures 8c and 8d).

The observed water mass transport on May 9 is close to zero (-0.05 Sv, Figure 7a) as currents from the mooring are weak (maximum speed of about 6 cm/s), directed northward at the surface and southward at depth (Figure 4). The same vertical shear is registered in the synthetic LIME-ROMS mooring (Figure 6) even though velocities are stronger (maximum speed of 25 cm/s). The model section through the Channel reveals that the strong vertical shear is also associated with a remarked horizontal across-channel variability (Figure 8c) due to surface cyclonic and anticyclonic features ex-

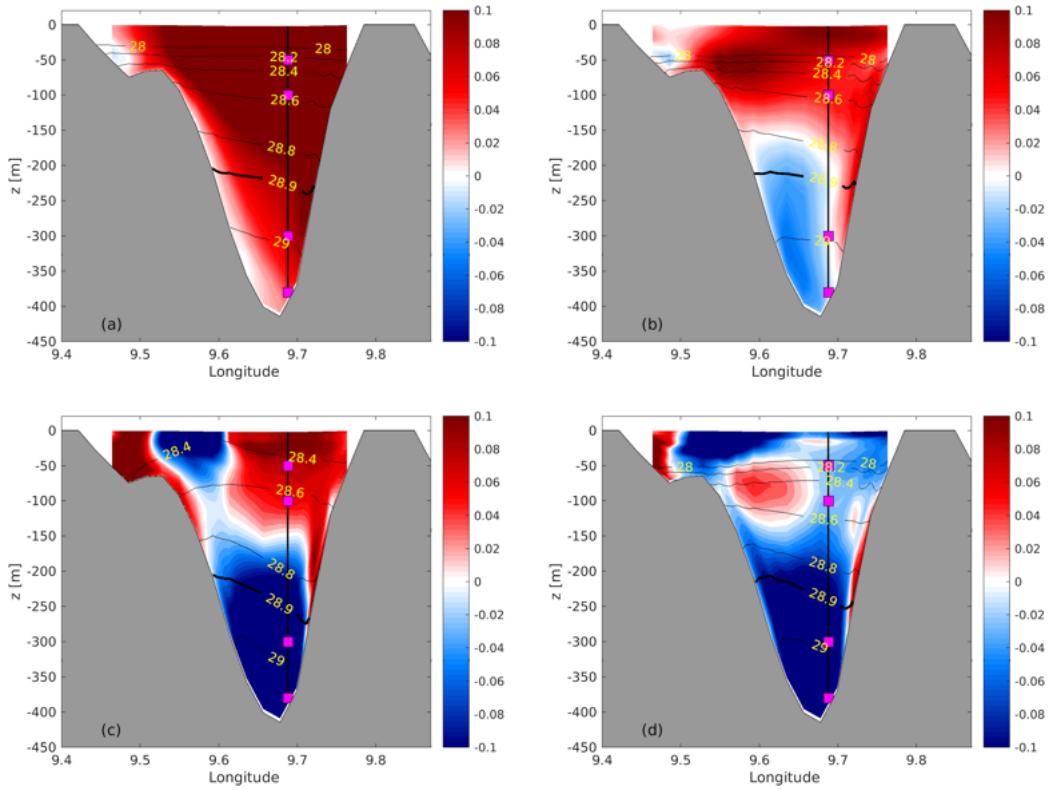

Figure 8: LIME-ROMS meridional velocities (m/s) inside the Corsica Channel. Black lines and yellow numbers indicate potential density contours (kg/m^3). (a) 2004 annual mean; (b) averaged over the period June 1 - September 30, 2004; (c) May 9 and (d) July 11, 2004.

tending down to a depth of 150 meters. The overall LIME-ROMS water mass transport for May 9 takes into account also the horizontal variability and is equal to -0.14 Sv.

The observed transport is minimum (-0.54 Sv) on July 11 (Figure 7a) when the flow is southward at all depths for the observed and synthetic moorings. Even on this day the model section shows across-channel variability (Figure 8d), with a subsurface positive core centered at 75 meters of depth while the flow is bottom-intensified at the mooring position. Due to the positive areas, the resulting LIME-ROMS transport for July 11 is less negative and equal to -0.29 Sv.

Figure 9 shows the Hovmöller diagram for the depth-integrated meridional velocity as a function of time and longitude in the Channel. The diagram confirms the importance of the across-channel variability throughout the entire 2004. It also points out three important results: First, the largest temporal variability is registered in the western flank of the Channel, near Corsica, where the flow reverses its northward direction more frequently. Second, only energetic episodes of current reversals reach the other flank of the Channel and may thus be seen by the mooring (black triangle in the upper part of Figure 9a). Moreover, it is worth pointing out that the mooring location at depth corresponds to the easternmost edge of the negative area of the averaged velocities in Figure 8b. Lastly, an important reversal is visible in the LIME-ROMS simulations on September 24, when the hydrographic data shown in Section 3.1 and in Figure 2 are available. All the information are used in the next section.

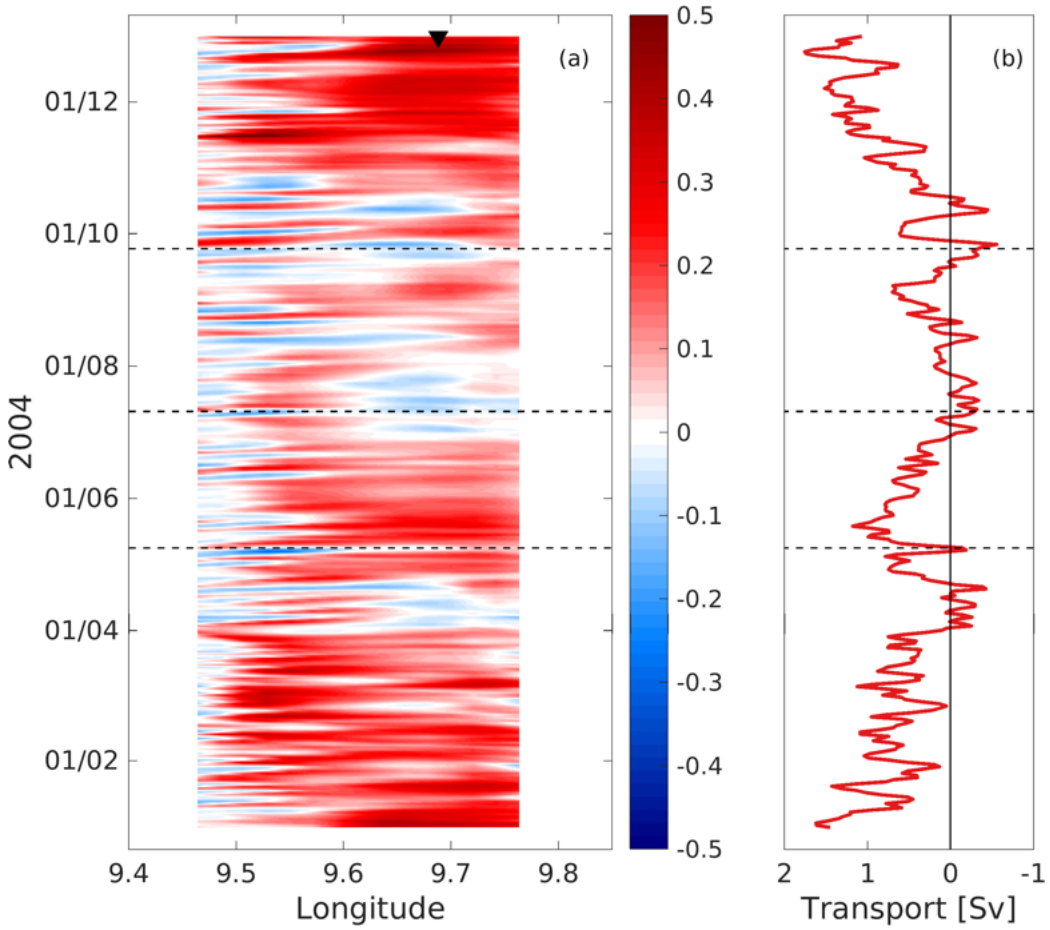

Figure 9: (a) Hovmöller diagram of the LIME-ROMS depth-averaged meridional velocities (m/s) as a function of time and longitude in the Corsica Channel. The black triangle lies on the longitude of the Corsica Channel mooring. (b) LIME-ROMS Corsica Channel water mass transport. Horizontal dashed lines indicate May 9, July 11 and September 24, 2004.

4. Discussion

Results from Section 3 give confidence in the LIME-ROMS setup around the Corsica Channel as the simulated fields are in good agreement with the observations in that area. The agreement gets worse when moving more southward in the Tyrrhenian Sea, as the LIME-ROMS model does not seem to reproduce properly some main features, like the summer position and size of the Bonifacio Cyclone. Nevertheless, LIME-ROMS results confirm the occurrence and the importance of flow reversals within the Corsica Channel, both in the observations and models. The high-resolution model shows current reversals with periodicity of the order of a few days to a week. They are more present in the western flank of the Channel and could be potentially missed by the real mooring located more toward the eastern flank of the same Channel. Vertical variability in the model velocity field persists at least at the seasonal scale (Figure 8b). On the contrary, the meridional velocity across-channel variability, evident for single reversal episodes, gets almost completely smeared out in the annual and seasonal averages (Figure 8). This explains the good agreement between observed and model annual transport values as the single mooring is adequate enough to capture the vertical variability in the Channel and the seasonal changes associated with it.

Having checked once again the realism of the LIME-ROMS setup, the rest of this section specifically aims at discussing the possible kinematic causes for the flow reversals with the help of the model.

We first look at wind forcing for the following multiple reasons: winds may directly affect the surface layers but also the whole water column through

the induced setup. Indeed, vertical coherent oscillations in the Channel at a 2.5-day periodicity have been associated with a setup forced by prevailing eastward winds (Manzella, 1985). In Pierini and Simioli (1998) the wind-driven transport through the Channel accounts for 15-40% of the observed values and wind fluctuations are proposed to explain current reversals over a period of a few days. In Pinardi and Masetti (2000) the Channel transport values are weak and not realistic if wind forcing is not used. Model results by Herbaut et al. (1997) suggest that changes in the Corsica Channel transport are linked only to winds and not to the density differences between the Tyrrhenian and Ligurian Seas.

To test this first hypothesis, 10 meters ERA-Interim zonal winds are averaged west of the tip of the Corsica Island (blue box in Figure 1b) where they are known to be among the strongest winds sweeping the central Ligurian Sea (see Figures 3 and 8 in Small et al. 2012). Furthermore, they are expected to be the most relevant from a dynamical point of view as flow reversals seem to arise from the western flank of the Channel (cf. the Hovmöller diagram in Figure 9 and text below).

The time evolution for the averaged winds is reported in Figure 7b. If compared with the curves for the transports (Figure 7a), one can immediately note that negative transport episodes are associated with peaks in wind speeds. Not all the high-wind speed events are associated with negative transports, however. Indeed, the water mass transport through the Channel is correlated with zonal wind speeds, with $r = 0.25$. This value is significant (95% significance level) but it does not explain the full variability of the water mass transport and the current reversals. We change the cor-

relation lag and the location and size of the area over which the average is performed but the correlation is weakly sensitive to these choices and never reaches values greater than $r = 0.30$.

Second, we test the hypothesis put forth by Ciuffardi et al. (2016) and dealing with the presence of the Ligurian anticyclone. According to Ciuffardi et al. (2016), the changes in its shape and location would favor the appearance of southern currents in the Corsica Channel. When the anticyclone is wide and located north or east of the Channel, no reversals can occur. On the other hand, when the anticyclone is small and displaced to the west of the Channel, a southward flow from the Ligurian Sea to the Tyrrhenian may be observed. We note that, in this case, the Ligurian anticyclone is centered around the Capraia Island as shown by drifters completing more loops around the island (Poulain et al., 2012). The descending southward branch of the anticyclone takes place east of Capraia (Ciuffardi et al., 2016, cf. their Figure 7), away from both real and synthetic moorings, as well as from the vertical sections of Figure 8. This is true in the model outputs of Onken et al. (2005, cf. their Figures 5 and 6), where an anticyclonic structure of about 40 km is reported as "Capraia eddy" and located in the area between the islands of Elba and Capraia and the Italian mainland.

Indeed most of the time, the Ligurian anticyclone in LIME-ROMS appears displaced east of Capraia, toward the coast of Tuscany and north of the Elba Island (cf. Figure 3b). At the same time, flow reversals may still occur as a southward flow is evident close to the western flank of the Corsica Channel. It may be then concluded that the presence of the Ligurian anticyclone is unlikely related to the current reversals found in the high-resolution

LIME-ROMS simulations.

Figure 3b shows that flow reversals in the LIME-ROMS are associated with a different circulation pattern. The WCC sharply veers right soon after the tip of the Corsica Island, flows into the Channel and keeps moving southward. Here we propose that, when this circulation pattern occurs, the meridional flow in the Corsica Channel can be tracked as characterized by colder and fresher Atlantic Waters brought by the WCC intrusions flowing toward the south (i.e. negative velocity). During this movement, WCC intrusions push the warmer saltier ECC waters toward the eastern flank of the Channel.

The analysis of the model results around September 24 confirms this hypothesis. As noted earlier in Section 3.1, on September 24, the LIME-ROMS salinity deep values in the Channel are lower than in the observations (Figure 2b, 10b). This apparent inconsistency is explained by the fact that, on September 24, LIME-ROMS fields are characterized by current reversals at all depths and negative transports close to the 2004 minimum value (cf. Figures 6 and 7a). No reversals are instead registered in the observations on the same day, when hydrographic data are taken: currents move northward, are weak at the surface (Figure 4) and the water mass transport is close to zero (Figure 7a). As currents reversals are limited in time, we may look at the LIME-ROMS salinity sections within the Channel on September 15 and October 1, i.e. on two moments before and after September 24 (Figure 10). On these days LIME-ROMS velocities are northward and LIME-ROMS transport is positive (vertical green lines in Figures 6 and 7a). As expected, the salinity values of the LIW waters at the bottom of the Channel are higher

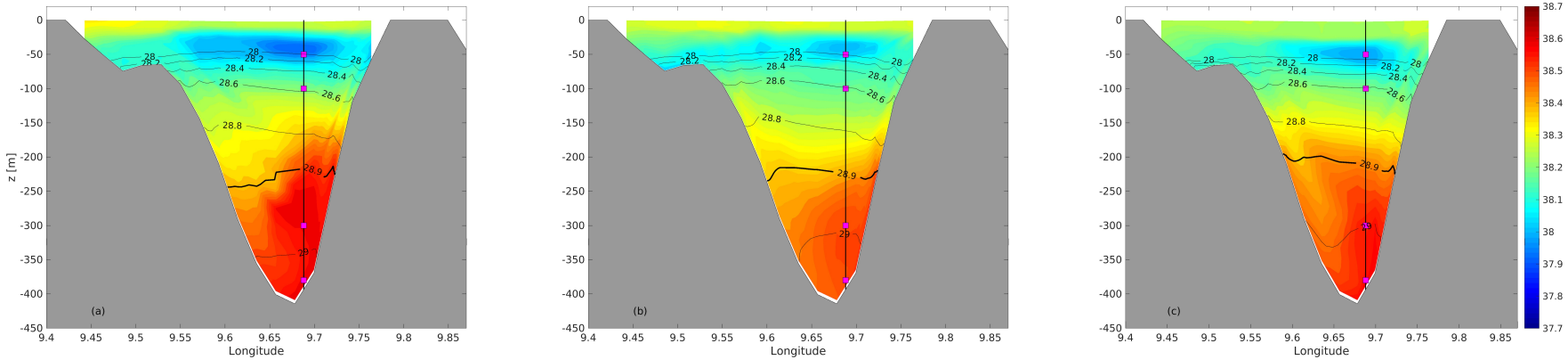

Figure 10: LIME-ROMS salinity sections within the Corsica Channel on (a) September 15, (b) September 24, and (c) October 1, 2004. Black lines indicate potential density contours (kg/m^3)

and closer to the observations, with values reaching 38.6 (Figure 10). We also point out that 2004 is an exceptionally salty year for the Mediterranean Sea (Borghini et al., 2014) and that these values are still saltier than the climatological range near the bottom of the Channel (38.55-38.56) reported for the 1995-2004 decade (World Ocean Atlas 2013, Zweng et al. 2013) .

The correlation between southward flows and lower salinity values at the bottom of the Corsica Channel is not limited on September 24 but found throughout the year. Figures 11a and 11b show composite pictures for velocities at 300m depth during negative/positive transport episodes, confirming the surface circulation pattern in the Corsica Channel shown in Figure 3. Negative transport episodes are associated with WCC intrusions in the Corsica Channel (Figure 11a) that, due to bathymetric constraints, occur further north compared to the surface circulation (Figure 3b). WCC intrusions bring fresher waters into the Corsica Channel (Figure 11c) if compared to positive transport episodes (Figures 11b and 11d).Similarly the time evolution of bottom salinity (Figure 7c), it is clear that lower salinity values are associated with negative transport episodes. Indeed, model velocities and salinities at the location of the deepest Corsica Channel current meter reach a correlation value of $r = 0.76$ (95% significance level). We summarize that WCC intrusions on the western flank of the Corsica Channel are responsible for flow reversals. Evidence of these intrusions can also be found in the literature. For example, currents are moving southward near the tip of Corsica in some of the numerical results presented in Figure 6 of Onken et al. (2005). A similar pattern can also be observed in the numerical results of Casella et al. (2011) (see their Figure 3). The satellite sea surface temperature snap-

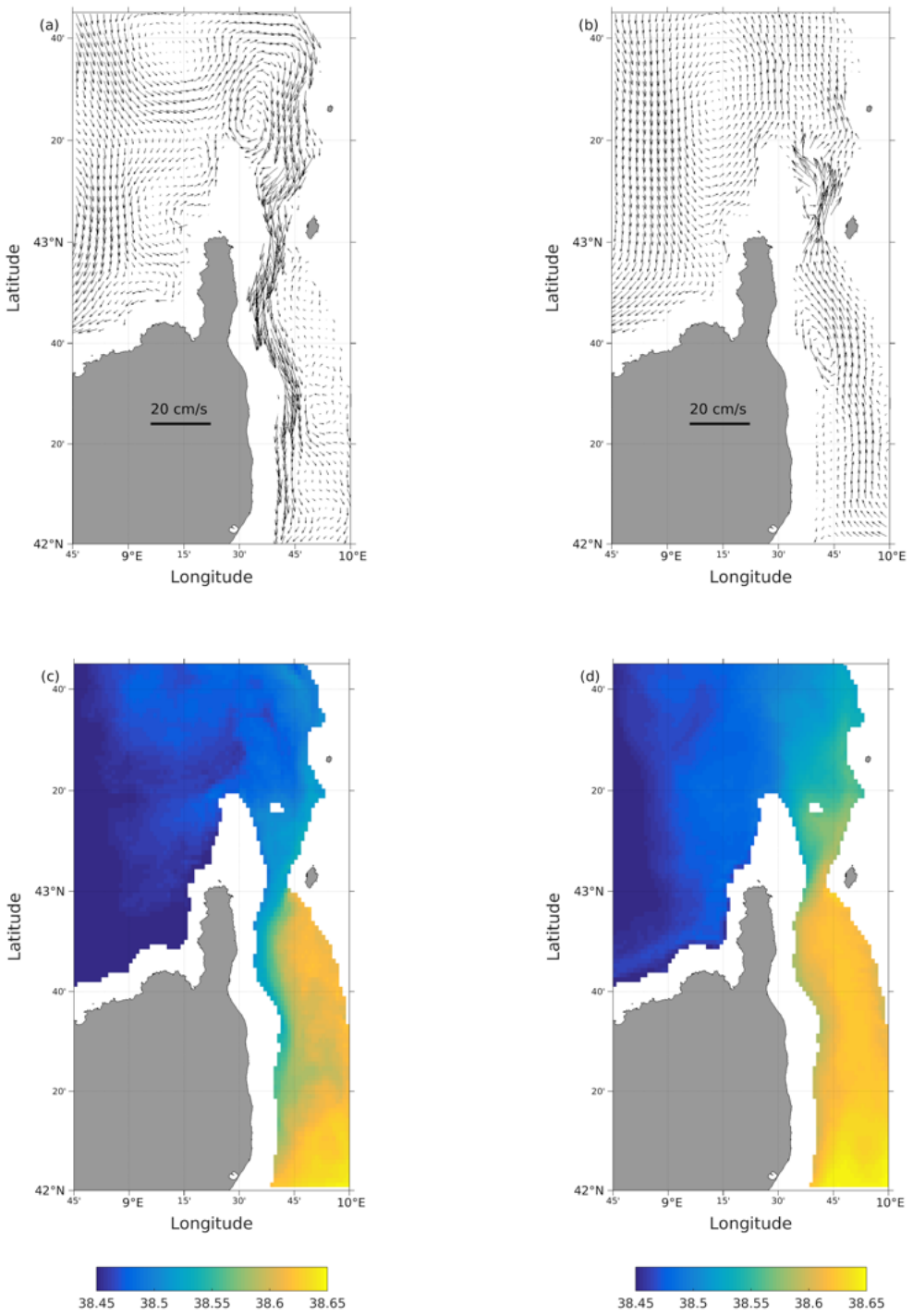

Figure 11: Composite of velocities and salinities at 300m depth for (a,c) negative and (b,d) positive transport episodes, representing reversal and normal conditions, respectively.

shot of Bouffard et al. (2008) (see their Figure 1) shows colder waters in the Channel which are in contiguity with the northwestern side of the Corsica Island. Similar satellite images can be obtained for episodes considered in this study, like for example for July 11, 2004 when the minimum transport value is observed (not shown). Nevertheless, none of these studies specifically remarks or points out either the WCC intrusions or the flow reversals in the Channel.

An important exception is one of the first observational efforts in the area reported in Stocchino and Testoni (1969) and later reproposed by Colacino et al. (1981) and Salusti and Travaglioni (1985). In their one-time experiment held in summer 1966 (June 13 - July 1), Stocchino and Testoni (1969) observed a prevalent northward current together with a complex interplay of flow structures with cyclonic and anticyclonic features interacting at different depths (cf. Figure 13 of Colacino et al. 1981). Near the tip of Corsica and along its coasts, they also observed a southward current extending at least down to 150 meters, i.e. to the maximum depth sampled by their deepest current meter.

As pointed out by Manzella (1985), the circulation depicted in Stocchino and Testoni (1969) was assumed not to be complete and verified by means of long-term current measurements. As a result, Stocchino and Testoni's findings, together with the first indications of WCC intrusions and associated reversals, have always been neglected so far.

5. Conclusions

In this study, results from a high-resolution ($\sim$ 1.5 km) LIME-ROMS numerical simulation of the area around the Corsica Channel during 2004 are presented. The focus is primarily on the current reversals within the Channel already present in past current meter observations (Vignudelli et al., 1999) and which have been poorly described from a kinematic point of view. This work provides a first synoptic view of these reversals during 2004.

The results show that the high-resolution LIME-ROMS model does not reproduce properly some main features of the general circulation like the Bonifacio cyclone but faithfully reproduces the qualitative state of the circulation in terms of general hydrographic structure and current variability observed within the Corsica Channel. In particular, good correspondence is found between the 2004 model annual water mass transport mean and standard deviation values of 0.49 ± 0.49 Sv and those estimated by observations and equal to 0.54 ± 0.50 Sv.

The numerical results reveal new important details of the high-frequency variability in the Corsica Channel. The high-resolution model shows that current reversals with periodicity of the order of a few days to a week, are more frequent near its western flank, in summer and early fall. The model also suggests that current reversals are associated with both horizontal and vertical shears due to the presence of both cyclonic and anticyclonic features in the Channel.

Contrary to the horizontal across-channel variability, the vertical variability in the model velocity field persists when the averages are performed at least at the seasonal scale. Thus, our results also show that the single

mooring assumption is adequate to capture the low-frequency and seasonal variability but question its adequacy for higher frequency signals. Results undermine the observational assumption that the across-channel variability of the meridional velocity is negligible for high-frequency signals as a single mooring may not be enough to fully capture the strong horizontal shears associated with flow reversals in the Channel. To this end, model results suggest that at least a second mooring should be put in place more toward the western flank of the Channel.

From a numerical point of view, our findings suggest that high (< 2 km) horizontal resolutions are needed to numerically resolve and capture the magnitude of the high-frequency reversals in the Channel. Lower resolutions yield transport values that are too low in terms of annual means and standard deviations. Furthermore, high-resolution models with open boundaries located at the Corsica Channel and using MFS outputs are not uncommon. Our results suggest that, at least for 2004, they may underestimate the effects due to the mean signals and the important high-frequency reversals coming from the Channel.

Our study addresses the variability and kinematics within the Corsica Channel. The role of current reversals in setting properties of the Ligurian Current and their controlling mechanisms are deferred to future work. Nevertheless, our results provide some dynamical insights. Models agrees with what was reported for the first time by Stocchino and Testoni (1969), i.e. that reversals start from the tip of the Corsica Island and are due to WCC intrusions into the Channel. Even if negative transport values are associated with peaks in wind speeds, there is no obvious relation between reversals

and zonal winds during 2004. Model current reversals are also not directly affected by the presence of the Ligurian anticyclone. Our results indicate that targeted field campaigns are needed to find further empirical evidence of the "Stocchino and Testoni's reversal currents".

Finally, this study is limited to the 2004 year and its implications will be checked in the future for other years. Future numerical simulations will be run for more recent years and more idealized setups will be considered to identify dynamical constraints for the Corsica Channel reversals.

Acknowledgments

This work was supported by the Italian Ministry of University and Research through the RITMARE Italian Flagship Project, and the IMPACT (PC IFM 2014-2020, Prot. ISMAR n. 0002269) and JERICO-NEXT (FP7, Grant number 654410) European projects. The authors would like to thank Mireno Borghini for providing technical assistance in the mooring deployment and in retrieving part of the data used in this work. The authors would like to thank the officers and crew members of the R/V Urania for providing continuous support during sea operations to collect the observational data used in this work.

References

Aliani, S., Meloni, R., 1999. Dispersal strategies of benthic species and water current variability in the Corsica channel (Western Mediterranean). Scientia Marina 63 (2), 137–145, doi:10.3989/scimar.1999.63n2137.

718 Aliani, S., Molcard, A., 2003. Hitch-hiking on floating marine debris: mac-
719 robenthic species in the Western Mediterranean Sea. Hydrobiologia 503 (1–
720 3), 59–67, doi:10.1023/B:HYDR.0000008480.95045.26.

721 Amante, C., Eakins, B. W., 2009. ETOPO1 1 Arc-minute global relief
722 model: procedures, data sources and analysis. NOAA Technical Memo-
723 randum NESDIS NGDC-24, National Geophysical Data Center, NOAA,
724 doi:10.7289/V5C8276M.

725 Artale, V., Astraldi, M., Buffoni, G., Gasparini, G., 1994. Seasonal variability
726 of gyre-scale circulation in the Northern Tyrrhenian sea. Journal of Geo-
727 physical Research: Oceans 99 (C7), 14127–14137, doi:10.1029/94JC00284.

728 Astraldi, M., Bianchi, C., Gasparini, G., Morri, C., 1995. Climatic fluctua-
729 tions, current variability and marine species distribution-a case-study in
730 the Ligurian sea (North-West Mediterranean). Oceanologica Acta 18 (2),
731 139–149, http://archimer.ifremer.fr/doc/00096/20768/.

732 Astraldi, M., Gasparini, G., 1992. The seasonal characteristics of the circu-
733 lation in the North Mediterranean basin and their relationship with the
734 atmospheric-climatic conditions. Journal of Geophysical Research: Oceans
735 97 (C6), 9531–9540, doi:10.1029/92JC00114.

736 Astraldi, M., Gasparini, G., Manzella, G., Hopkins, T., 1990. Temporal vari-
737 ability of currents in the Eastern Ligurian Sea. Journal of Geophysical
738 Research: Oceans 95 (C2), 1515–1522, doi:10.1029/JC095iC02p01515.

739 Astraldi, M., Gasparini, G. P., 1990. Influence of the climatic conditions
740 on the winter fluxes in the Corsican Channel. In: Pratt L.J. (eds) The

741 Physical Oceanography of Sea Straits. NATO ASI Series (Mathematical
742 and Physical Sciences), vol 318. Springer, Dordrecht, doi:10.1007/978-94-
743 009-0677-8_9.

744 Astraldi, M., Gasparini, G. P., 2013. The Seasonal Characteristics of the
745 Circulation in the Tyrrhenian Sea. In Seasonal and Interannual Vari-
746 ability of the Western Mediterranean Sea, P. E. La Viollette (Ed.).
747 doi:10.1029/CE046p0115.

748 Blayo, E., Debreu, L., 2005. Revisiting open boundary conditions from
749 the point of view of characteristic variables. Ocean Modell. 9, 231–252,
750 doi:10.1016/j.ocemod.2004.07.001.

751 Borghini, M., Bryden, H., Schroeder, K., Sparnocchia, S., Vetrano, A., 2014.
752 The Mediterranean is becoming saltier. Ocean Science 10 (4), 693–700,
753 doi:10.5194/os-10-693-2014.

754 Bouffard, J., Vignudelli, S., Cipollini, P., Menard, Y., 2008. Exploiting the
755 potential of an improved multimission altimetric data set over the coastal
756 ocean. Geophysical Research Letters 35 (10), doi:10.1029/2008GL033488.

757 Canuto, V. M., Howard, A., Cheng, Y., Dubovikov, M. S., 2001. Ocean
758 turbulence, Part I: one-point closure model momentum and heat ver-
759 tical diffusivities. J. Phys. Oceanogr. 31, 1413–1426, doi:10.1175/1520-
760 0485(2001)031<1413:OTPIOP>2.0.CO;2.

761 Carniel, S., Warner, J. C., Chiggiato, J., Sclavo, M., 2009. Investigating the
762 impact of surface wave breaking on modeling the trajectories of drifters

763 in the Northern Adriatic Sea during a wind-storm event. Ocean Modelling
764 30 (2), 225–239, doi:10.1016/j.ocemod.2009.07.001.

765 Casella, E., Molcard, A., Provenzale, A., 2011. Mesoscale vortices in the
766 Ligurian Sea and their effect on coastal upwelling processes. Journal of
767 Marine Systems 88 (1), 12–19, doi:10.1016/j.jmarsys.2011.02.019.

768 Chapman, D. C., 1985. Numerical treatment of cross-shelf open boundaries
769 in a barotropic coastal ocean model. J. Phys. Oceanogr. 15 (3), 1060–1075,
770 doi:10.1175/1520-0485(1985)015<1060:NTOCSO>2.0.CO;2.

771 Chiggiato, J., Oddo, P., 2008. Operational ocean models in the Adriatic Sea:
772 a skill assessment. Ocean Sci. 4, 61–71, doi:10.5194/os-4-61-2008.

773 Ciuffardi, T., Napolitano, E., Iacono, R., Reseghetti, F., Raiteri, G., Bor-
774 done, A., 2016. Analysis of surface circulation structures along a frequently
775 repeated XBT transect crossing the Ligurian and Tyrrhenian seas. Ocean
776 Dynamics 66 (6-7), 767–783, doi:10.1007/s10236-016-0954-y.

777 Colacino, M., Garzoli, S., Lop-Museum, Salusti, E., Mar 1981. Currents and
778 countercurrents in the Western Mediterranean straits. Il Nuovo Cimento
779 C 4 (2), 123–144, doi:10.1007/BF02507396.

780 Crépon, M., Wald, L., Monget, J.-M., 1982. Low-frequency waves in the Lig-
781 urian sea during december 1977. Journal of Geophysical Research: Oceans
782 87 (C1), 595–600, doi:10.1029/JC087iC01p00595.

783 Damien, P., Bosse, A., Testor, P., Marsaleix, P., Estournel, C., 2017. Mod-
784 eling postconvective submesoscale coherent vortices in the Northwestern

785 Mediterranean Sea. Journal of Geophysical Research: Oceans, 122,9937-
786 9961, doi:10.1002/2016JC012114.

787 Dee, D. P., Uppala, S. M., Simmons, A. J., Berrisford, P., Poli, P., Kobayashi,
788 S., Andrae, U., Balmaseda, M. A., Balsamo, G., Bauer, P., Bechtold, P.,
789 Beljaars, A. C. M., van de Berg, L., Bidlot, J., Bormann, N., Delsol,
790 C., Dragani, R., Fuentes, M., Geer, A. J., Haimberger, L., Healy, S. B.,
791 Hersbach, H., Hólm, E. V., Isaksen, L., Kållberg, P., Köhler, M., Ma-
792 tricardi, M., McNally, A. P., Monge-Sanz, B. M., Morcrette, J.-J., Park,
793 B.-K., Peubey, C., de Rosnay, P., Tavolato, C., Thépaut, J.-N., Vitart, F.,
794 2011. The ERA-INTERIM reanalysis: configuration and performance of
795 the data assimilation system. Q. J. R. Meteorol. Soc. 137 (656), 553–597,
796 doi:10.1002/qj.828.

797 Delrosso, D., Clementi, E., Grandi, A., Tonani, M., Oddo, P., Girardi Fer-
798 uzza, G., Pinardi N., 2016. Towards the Mediterranean Forecasting Sys-
799 tem MyOcean V5: numerical experiments results and validation. 345,
800 http://hdl.handle.net/2122/11435.

801 Dobricic, S., Pinardi, N., 2008. An oceanographic three-dimensional vari-
802 ational data assimilation scheme. Ocean modelling 22 (3), 89–105,
803 doi:10.1016/j.ocemod.2008.01.004.

804 Echevin, V., Crépon, M., Mortier, L., 2003. Simulation and analysis of the
805 mesoscale circulation in the Northwestern Mediterranean Sea. Annales
806 Geophysicae 21 (1), 281–297, doi:10.5194/angeo-21-281-2003.

807 Fairall, C. W., Bradley, E. F., Godfrey, J. S., Wick, G. A., Edson, J. B.,

Young, G. S., 1996a. Cool-skin and warm-layer effects on sea surface temperature. J. Geophys. Res. 101 (C1), 1295–1308, doi:10.1029/95JC03190.

Fairall, C. W., Bradley, E. F., Rogers, D. P., Edson, J. B., Young, G. S., 1996b. Bulk parameterization of air-sea fluxes for Tropical Ocean-Global Atmosphere Coupled-Ocean Atmosphere Response Experiment. J. Geophys. Res. 101 (C2), 3747–3764, doi:10.1029/95JC03205.

Fernández, V., Dietrich, D. E., Haney, R. L., Tintoré, J., 2005. Mesoscale, seasonal and interannual variability in the Mediterranean Sea using a numerical ocean model. Progress in Oceanography 66 (2), 321–340, doi:10.1016/j.pocean.2004.07.010.

Fossi, M. C., Romeo, T., Baini, M., Panti, C., Marsili, L., Campani, T., Canese, S., Galgani, F., Druon, J.-N., Airoldi, S., et al., 2017. Plastic debris occurrence, convergence areas and fin whales feeding ground in the Mediterranean marine protected area Pelagos Sanctuary: A modeling approach. Frontiers in Marine Science 4, 167, doi:10.3389/fmars.2017.00167.

Garrett, C., MacCready, P.,Rhines, P., 1993. Boundary Mixing and Arrested Ekman Layers: Rotating Stratified Flow Near a Sloping Boundary. Annual Review of Fluid Mechanics 25 (1), 291–323, doi:10.1146/annurev.fl.25.010193.001451.

Gasparini, G., Manzella, G., 1983. A possible eddy generating mechanism in the Ligurian basin. Applied Mathematical Modelling 7 (4), 291–294, doi:10.1016/0307-904X(83)90086-0.

Haidvogel, D. B., Arango, H. G., Hedstrom, K., Beckmann, A., Malanotte-Rizzoli, P., Shchepetkin, A. F., 2000. Model evaluation experiments in the North Atlantic Basin: simulations in nonlinear terrain-following coordinates. Dyn. Atmos. Oceans 32 (3-4), 239–281, doi:10.1016/S0377-0265(00)00049-X.

Haidvogel, D. B., Beckmann, A., 1999. Numerical Ocean Circulation Modeling. Imperial College Press, 344 pp., ISBN: 1-86094-114-1.

Herbaut, C., Martel, F., Crépon, M., 1997. A sensitivity study of the general circulation of the Western Mediterranean Sea. part II: the response to atmospheric forcing. Journal of Physical Oceanography 27 (10), 2126–2145, doi:10.1175/1520-0485(1997)027<2126:ASSOTG>2.0.CO;2.

Iermano, I., Moore, A. M., Zambianchi, E., 2016. Impacts of a 4-dimensional variational data assimilation in a coastal ocean model of Southern Tyrrhenian Sea. J. Mar. Sys. 154, Part B, 157–171, doi:10.1016/j.jmarsys.2015.09.006.

Ilıcak, M., Adcroft, A. J., Griffies, S. M., Hallberg, R. W., 2012. Spurious dianeutral mixing and the role of momentum closure. Ocean Modelling. 45–46, 37–58, https://doi.org/10.1016/j.ocemod.2011.10.003

Ilıcak, M., Özgókmen, T. M., Peters, H., Baumert, H. Z., Iskandarani, M., 2008. Performance of two-equation turbulence closures in three-dimensional simulations of the Red Sea overflow. Ocean Modelling. 24,3-4, 122–139, https://doi.org/10.1016/j.ocemod.2008.06.001.

852 Madec, G., Delécluse, P., Imbard, M., Lévy, C., 1998. OPA 8.1 Ocean General
853 Circulation Model reference manual, https://hal.archives-ouvertes.
854 fr/hal-00154217.

855 Magaldi, M. G., Özgökmen, T. M., Griffa, A., Rixen, M., 2010. On
856 the response of a turbulent coastal buoyant current to wind events:
857 the case of the Western Adriatic Current. Ocean Dyn. 60 (1), 93–122,
858 doi:10.1007/s10236-009-0247-9.

859 Manzella, G., 1985. Fluxes across the corsica channel and coastal circulation
860 in the East Ligurian Sea, Northwestern Mediterranean. Oceanologica Acta
861 8 (1), 29–35, http://archimer.ifremer.fr/doc/00112/22317/.

862 Marullo, S., Santoleri, R., Bignami, F., 2013. The Surface Characteris-
863 tics of the Tyrrhenian Sea: Historical Satellite Data Analysis. Ameri-
864 can Geophysical Union (AGU), Ch. 8, pp. 135–154, https://agupubs.
865 onlinelibrary.wiley.com/doi/abs/10.1029/CE046p0135

866 Millot, C., 1999. Circulation in the Western Mediterranean sea. Journal of
867 Marine Systems 20 (1), 423–442, doi:10.1016/S0924-7963(98)00078-5.

868 Moen, J., 1984. Variability and mixing of the surface layer in the Tyrrhenian
869 Sea. milex-80. Tech. rep., SACLANT ASW RESEARCH CENTRE La
870 Spezia (Italy), http://www.dtic.mil/dtic/tr/fulltext/u2/a141929.
871 pdf.

872 Mounier, F., Echevin, V., Mortier, L., Crepon, M., 2005. Analysis of the
873 mesoscale circulation in the occidental Mediterranean sea during winter

1999–2000 given by a regional circulation model. Progress in Oceanography 66 (2), 251–269, doi:10.1016/j.pocean.2004.11.003.

Myers, P. G., Haines, K., 2000. Seasonal and interannual variability in a model of the Mediterranean under derived flux forcing. Journal of physical oceanography 30 (5), 1069–1082, doi:10.1175/1520-0485(2000)030<1069:SAIVIA>2.0.CO;2.

Onken, R., 2017. Validation of an ocean shelf model for the prediction of mixed-layer properties in the Mediterranean Sea West of Sardinia. Ocean Science 13 (2),235–257, doi:10.5194/os-13-235-2017.

Onken, R., Robinson, A. R., Kantha, L., Lozano, C. J., Haley, P. J., Carniel, S., 2005. A rapid response nowcast/forecast system using multiply nested ocean models and distributed data systems. Journal of Marine Systems 56 (1-2), 45–66, doi:10.1016/j.jmarsys.2004.09.010.

Pierini, S., Simioli, A., 1998. A wind-driven circulation model of the Tyrrhenian Sea area. Journal of Marine Systems 18 (1-3), 161–178, doi:10.1016/S0924-7963(98)00010-4.

Pinardi, N., Masetti, E., 2000. Variability of the large scale general circulation of the Mediterranean Sea from observations and modelling: a review. Palaeogeography, Palaeoclimatology, Palaeoecology 158 (3-4), 153–173, doi:10.1016/S0031-0182(00)00048-1.

Poulain, P.-M., Gerin, R., Rixen, M., Zanasca, P., Teixeira, J., Griffa, A., Molcard, A., Marte, M., Pinardi, N., 2012. Aspects of the surface circulation in the Liguro-Provençal basin and Gulf of Lion as observed by

satellite-tracked drifters (2007-2009). Bollettino di Geofisica Teorica ed Applicata 53 (2), 261–279, doi:10.4430/bgta0052.

Rinaldi, E., Buongiorno Nardelli, B., Zambianchi, E., Santoleri, R., Poulain, P.-M., 2010. Lagrangian and Eulerian observations of the surface circulation in the Tyrrhenian Sea. Journal of Geophysical Research: Oceans 115 (C4), doi:10.1029/2009JC005535.

Salusti, E., Travaglioni, F., 1985. Currents and countercurrents in straits. Oceanologica Acta 8 (2), 197–206, http://archimer.ifremer.fr/doc/00112/22306/.

Schroeder, K., Chiggiato, J., Bryden, H., Borghini, M., Ismail, S. B., 2016. Abrupt climate shift in the Western Mediterranean sea. Scientific Reports 6, 23009, doi:10.1038/srep23009.

Schroeder, K., Josey, S., Herrmann, M., Grignon, L., Gasparini, G., Bryden, H., 2010. Abrupt warming and salting of the Western Mediterranean deep water after 2005: Atmospheric forcings and lateral advection. Journal of Geophysical Research: Oceans 115, C08029, doi:10.1029/2009JC005749.

Shchepetkin, A. F., McWilliams, J. C., 1998. Quasi-monotone advection schemes based on explicit locally adaptive dissipation. Mon. Weather Rev. 126 (6), 1541–1580, doi:10.1175/1520-0493(1998)126<1541:QMASBO>2.0.CO;2.

Shchepetkin, A. F., McWilliams, J. C., 2005. The regional oceanic modeling system (ROMS): a split-explicit, free-surface, topography-

following-coordinate oceanic model. Ocean Modell. 9 (4), 347–404, doi:10.1016/j.ocemod.2004.08.002.

Small, R., Carniel, S., Campbell, T., Teixeira, J., Allard, R., 2012. The response of the Ligurian and Tyrrhenian Seas to a summer mistral event: A coupled atmosphere–ocean approach. Ocean Modelling 48, 30–44, doi:10.1016/j.ocemod.2012.02.003.

Stocchino, C., Testoni, A., 1969. Le correnti nel canale di Corsica e nell'arcipelago toscano. Comm. Ital. Oceanogr. 827 (A), 19.

Suaria, G., Aliani, S., 2014. Floating debris in the Mediterranean sea. Marine pollution bulletin 86 (1-2), 494–504, doi:10.1016/j.marpolbul.2014.06.025.

Suaria, G., Avio, C. G., Mineo, A., Lattin, G. L., Magaldi, M. G., Belmonte, G., Moore, C. J., Regoli, F., Aliani, S., 2016. The Mediterranean plastic soup: synthetic polymers in Mediterranean surface waters. Scientific reports 6, 37551, doi:10.1038/srep37551.

Umlauf, L., Burchard, H., 2003. A generic length-scale equation for geophysical turbulence models. J. Marine Res. 61, 235–265, doi:10.1357/002224003322005087.

Vetrano, A., Napolitano, E., Iacono, R., Schroeder, K., Gasparini, G., 2010. Tyrrhenian sea circulation and water mass fluxes in spring 2004: Observations and model results. Journal of Geophysical Research: Oceans 115,C06023, doi:10.1029/2009JC005680.

Vignudelli, S., Cipollini, P., Astraldi, M., Gasparini, G. P., Manzella,

941 G., 2000. Integrated use of altimeter and in situ data for under-
942 standing the water exchanges between the Tyrrhenian and Ligurian
943 Seas. Journal of Geophysical Research: Oceans 105 (C8), 19649–19663,
944 doi:10.1029/2000JC900083.

945 Vignudelli, S., Cipollini, P., Roblou, L., Lyard, F., Gasparini, G. P.,
946 Manzella, G., Astraldi, M., 2005. Improved satellite altimetry in coastal
947 systems: Case study of the Corsica channel (Mediterranean Sea). Geo-
948 physical Research Letters 32 (7), L07608, doi:10.1029/2005GL022602.

949 Vignudelli, S., Gasparini, G., Astraldi, M., Schiano, M.E., 1999. A possi-
950 ble influence of the North Atlantic Oscillation on the circulation of the
951 Western Mediterranean Sea. Geophysical Research Letters 26 (5), 623–
952 626, doi:10.1029/1999GL900038.

953 Warner, J. C., Sherwood, C. R., Arango, H. G., Signell, R. P.,
954 2005. Performance of four turbulence closure methods implemented
955 using a generic length scale method. Ocean Modell. 8, 81–113,
956 doi:10.1016/j.ocemod.2003.12.003.

957 Worley, S. J., Woodruff, S. D., Reynolds, R. W., Lubker, S. J., Lott, N., 2005.
958 ICOADS release 2.1 data and products. Int. J. Climatol 25 (7), 823–842,
959 doi:10.1002/joc.1166.

960 Zweng, M.M, Reagan, J.R., Antonov, J.I., Locarnini, R.A., Mis-
961 honov, A.V., Boyer,T.P., Garcia,H.E., Baranova,O.K.,Johnson,D.R., Sei-
962 dov,D.,Biddle,M.M., 2013. World Ocean Atlas 2013, volume 2: Salinity.

963 S.Levitus,Ed., Mishonov, Technical Ed., NOAA atlas NESDIS, vol. 74. 39
964 pp, https://data.nodc.noaa.gov/woa/WOA13/DOC/woa13_vol2.pdf.